https://doi.org/10.5194/egusphere-2026-4910
Preprint. Discussion started: 15 September 2026

Grain Size Distributions-Informed Extension of Turbidity–Suspended Sediment Concentration Relationships in a Glacier Basin

Chao Liu[1, 2, 3], Fan Zhang[2, 3, 4], Chen Zeng[2, 3, 5], Shichang Kang[3, 4]

[1] School of Geography and Environment, Liaocheng University, Liaocheng, Shandong 252059, China

[2] ECMI Team, State Key Laboratory of Tibetan Plateau Earth System Science, Resources and Environment (TPESRE), Institute of Tibetan Plateau Research, Chinese Academy of Sciences (CAS), Beijing 100101, China

[3] University of Chinese Academy of Sciences, Beijing 100101, China

[4] Institute of Mountain Hazards and Environment, Chinese Academy of Sciences, Chengdu 610213, China

[5] Lhasa Earth System Multi-Dimension Observatory Network (LEMON), Lhasa 850000, China

Correspondence to: Fan Zhang (zhangfan@itpcas.ac.cn)

Abstract

Fluvial sediment changes in cold regions are key research focus under global warming. However, the understanding in glacier basins remains constrained by sparse observations. Accurate turbidity–suspended sediment concentration (SSC) relationships are essential but challenging for real-time monitoring of SSC, especially in basins supplied by multi-source runoff. In this study, in-situ turbidity monitoring and SSC sampling were conducted at two cross sections, the Kuoqionggangri glacier terminus and the basin outlet, respectively. The main controls on turbidity–SSC relationships were examined via laboratory mixing experiments. Contrasts in sediment grain size distributions, shaped by varied sediment source zones during periods

https://doi.org/10.5194/egusphere-2026-4910
Preprint. Discussion started: 15 September 2026

dominated by snowmelt, glacier melt, and rainfall, respectively, are the primary driver of turbidity–SSC relationship variability. Relative to a full-period curve, period-specific curves improved the fit markedly, with R^2 increasing from 0.86 to 0.98. However, direct extrapolation of low-turbidity curves (<1400 NTU) to the medium range (1400~3000 NTU) performed poorly (NSE=-0.67~0.11). In contrast, extrapolation of grain-size composition achieved much higher accuracy (NSE=0.91~0.98). A grain-size informed framework was therefore developed to extend turbidity–SSC relationships by tracking systematic changes in grain-size fractions. SSC estimates for the medium-turbidity range derived using this framework achieved NSE values of 0.96~0.98, allowing the relationships to be extended from the sampled range (<2840 NTU) to an unsampled high-turbidity range (<5580 NTU). The framework provides a feasible approach for deriving high temporal resolution SSC from turbidity records in remote glacier basins and improves process-based understanding of sediment dynamics in high altitude or latitude rivers.

Keywords: Turbidity–SSC relationship; Sediment grain size; Multi-source runoff; Glacier basin; Tibetan Plateau.

1 Introduction

Long term and continuous monitoring of sediment concentration in rivers fed by multiple runoff sources is essential for comprehensively understanding sediment transport processes and for reliably quantifying riverine sediment loads (Hoffmann et al., 2020; Liu et al., 2023). Suspended sediment is commonly the dominant mode of fluvial sediment transport, accounting for more than 90% of the total sediment load in many river systems (Mieras et al., 2019), and serves as the principal carrier of nutrients, pollutants, and other particle-bound constituents in aquatic environments (Zeng et al., 2023). Accurate estimation and interpretation of suspended sediment loads are therefore critical for assessing erosion (Li et al., 2021a), channel siltation and

https://doi.org/10.5194/egusphere-2026-4910
Preprint. Discussion started: 15 September 2026

deposition (Li et al., 2021b), riverbed geomorphology (Yan et al., 2025), and water quality dynamics (Wu et al., 2026), all of which are crucial to basin management. Globally, river sediment loads have been profoundly reshaped by the combined effects of climate change and human activities (Delaney et al., 2025; Dethier et al., 2025). Rising temperatures, increasing precipitation, and land use change can enhance sediment supply (Knight and Harrison, 2009; Zhang et al., 2022a; Li et al., 2025), whereas dams and river regulation trap sediment and reduce downstream and coastal delivery (Wu et al., 2026). These interacting pressures are particularly pronounced in High Mountain Asia, where warming-induced hydrological shifts and intensified glacier melt contribute substantially to sediment production and export (Zhang et al., 2022b; Li et al., 2021a). Nevertheless, constrained by the complexity of hydrological–sediment processes and limitations in observation techniques, monitoring in glacier basins remains sparse, severely constraining process-based understanding of sediment dynamics and their responses to ongoing climate change.

In recent decades, the use of turbidity sensors to monitor suspended sediment loads has attracted increasing attention worldwide (Chauché et al., 2014; Chen et al., 2016; Droujko and Molnar, 2022). Turbidity, widely adopted as a surrogate for suspended sediment concentration (SSC) (Jalón-Rojas et al., 2015), is defined as the degree to which suspended particles scatter light in water and is expressed in nephelometric turbidity units (NTU) (Gippel, 1995; Downing, 2006; Gray and Gartner, 2009; Voichick et al., 2018; Mathers et al., 2019; Davies-Colley et al., 2021). In situ deployment of turbidity sensors enables real-time acquisition of high temporal resolution data (Chung et al., 2007; Davies-Colley et al., 2014), from which SSC can be estimated after calibration. Compared with traditional filtration and gravimetric approach, turbidity monitoring is more efficient and less constrained by sampling frequency, site accessibility, and observation duration. It has therefore been widely applied in lakes, low- to mid-elevation basins, and estuaries

https://doi.org/10.5194/egusphere-2026-4910
Preprint. Discussion started: 15 September 2026

(Walling et al., 1999; Jalón-Rojas et al., 2015; Skarbøvik et al., 2023; Wang et al., 2026). Because turbidity records must generally be calibrated against measured SSC, periodic water sampling remains necessary to establish appropriate turbidity–SSC relationships (Ziegler et al., 2014). Cross-basin comparisons have shown that turbidity–SSC regressions can differ markedly among river basins, indicating limited transferability (Bright and Mager, 2020; Skarbøvik et al., 2023), and controlled laboratory experiments have reached similar conclusions (Bakker et al., 2024; Ravazzolo et al., 2026). Collectively, these studies indicate that establishing an accurate, basin-specific turbidity–SSC relationship is a prerequisite for converting turbidity observations into reliable SSC estimates, and that such relationships often require separate calibration for different periods (Skarbøvik et al., 2023). This is because turbidity is controlled not only by SSC itself (Downing, 2006; Choi et al., 2024), but also by particle size (Druine et al., 2018), organic-matter content (Bright et al., 2020), density (Bilotta and Brazier, 2008), particle shape (Felix et al., 2018; Woźniak and Pisarska-Jamroży, 2018), and color (Sutherland et al., 2000). These factors c are the principal sources of uncertainty in turbidity–SSC relationships (Navratil et al., 2011; Bright et al., 2020).

Field sampling combined with laboratory experiments has been widely used to examine the controls on turbidity–SSC relationships under controlled conditions (Clifford et al., 1995; Davies-Colley and Smith, 2001; Murillo-Bermúdez et al., 2021). For example, Sehgal et al. (2022) developed a generalized turbidity–SSC formulation by incorporating median grain size (D_{50}), organic matter content, and particle-scattering efficiency, and validated it experimentally. This generalized equation quantitatively captures the influence of several key factors, giving it relatively broad applicability, while highlighting the dominant role of grain size and demonstrating its validity under low-sediment conditions. However, reliance on median grain size alone may

https://doi.org/10.5194/egusphere-2026-4910
Preprint. Discussion started: 15 September 2026

obscure important diagnostic information contained within the full particle size distribution (Chung, 2008). In recent years, an expanding body of research has further identified grain-size distribution as the dominant control on turbidity–SSC relationships (Druine et al., 2018; Landers et al., 2013; Pfannkuche and Schmidt 2003). Kim et al. (2025) developed turbidity–SSC relationships applicable across a broad range of suspended-sediment size fractions intended to reflect natural river conditions, while limited sampling frequency and spatial representativeness still hindered accurate calibration during extreme floods and typhoon-driven events. Despite these advances, a mature and practically applicable framework remains lacking for constructing and extending turbidity–SSC relationships in alpine basins under multi-source runoff conditions.

Up to date, most turbidity–SSC studies have focused on rivers with relatively simple or largely single-source sediment supplies (Potes et al., 2012; Sherriff et al., 2015), whereas glacier basins have received less attention despite their more complex suspended sediment provenance. For example, Chen et al. (2016) employed turbidity observations for short-term monitoring and analysis of SSCs in a glacier basin draining to Lake Nam Co on the Tibetan Plateau, but did not examine differences among hydrological periods. Sediment-source tracing in the Kuoqionggangri Glacier Basin further reveals a distinctly multi-source sediment regime: approximately 52.8% of sediment loads are derived from the glacial zone, whereas the remainder is supplied by overland erosion driven by snowmelt and rainfall, with bare land and meadow areas contributing about 40.7% and 6.5%, respectively (Liu et al., 2025). Such multi-source sediment supply remains poorly represented in existing turbidity–SSC studies. Moreover, SSCs reported in many previous turbidity–SSC studies are generally low, commonly <0.5 kg/m^3 (Sherriff et al., 2015), whereas SSCs in glacier basins can reach ~20 kg/m^3. This contrast reflects substantial differences in grain-size distributions, mineral composition, and hydrological regimes between glacier basins and

https://doi.org/10.5194/egusphere-2026-4910
Preprint. Discussion started: 15 September 2026

lower-elevation river systems. Under these complex and high sediment conditions, turbidity–SSC relationships may behave complicatedly, underscoring the need for targeted investigations tailored to these environments.

The primary aim of this study is to establish robust turbidity–SSC conversion relationships for a glacier basin and thereby enable high temporal resolution monitoring of SSC from turbidity records. Specifically, it is intended to (1) determine, on the basis of field observations, whether turbidity–SSC relationships differ among melt-dominated and rainfall-dominated periods; (2) identify the dominant controls on these relationships via laboratory mixing experiments that isolate the effects of suspended-sediment properties; and (3) integrate field monitoring with controlled laboratory mixing experiments to validate and extend turbidity–SSC relationships beyond the range constrained by discrete field sampling, particularly under high-turbidity conditions associated with extreme sediment concentrations. Collectively, these efforts are expected to advance mechanistic understanding of turbidity–SSC relationships and their governing factors in glacier basins, thereby providing a process-based framework for continuous sediment transport monitoring and for assessing sediment dynamics and their sensitivity to ongoing climate change in high-altitude or latitude cold region rivers.

2 Method and materials

2.1 Field sites

In this study, the Kuoqionggangri Glacier Basin is selected as a representative glacier basin on the southern Tibetan Plateau, characterized by distinct melt- and rainfall-driven hydrological regimes and vigorous sediment production typical of high-altitude glacier systems. Favorable conditions for sustained observation are provided by relatively convenient access and by the Lhasa observation platform, which supports well instrumented monitoring cross sections at the glacier

https://doi.org/10.5194/egusphere-2026-4910
Preprint. Discussion started: 15 September 2026

terminus and the basin outlet, thereby enabling continuous in situ turbidity measurements and routine SSC sampling despite harsh alpine conditions. Under ongoing climate change, the basin has exhibited dramatic environmental changes, including rapid warming and accelerated glacial ablation. It exhibits clearly defined snowmelt, glacier melt, and rainfall periods. In such settings, runoff borne sediment can respond rapidly to hydrological events driven by snowmelt, glacier melt, and rainfall (Petts et al., 1985; Old et al., 2005; Kaless et al., 2024), while sediment sources vary substantially across seasons and event types (Liu et al., 2025). This combination of strong hydroclimatic forcing, dynamic sediment supply, and relatively robust monitoring infrastructure renders the basin an ideal natural laboratory for evaluating turbidity–based frameworks in glacial environments.

For turbidity monitoring in the glacier basin, long range, real time telemetered turbidity monitoring systems were installed at two hydrological cross sections: the glacier terminus at 5316.8 m a.s.l and the basin outlet at 4905.5 m a.s.l, within the Kuoqionggangri Glacier Basin (90°12′0″E, 29°54′0″N) established by the Lhasa Earth System Multi-Dimensional Observatory Network (LESMDON) (Fig. 1). Background information for the basin is provided in Liu et al. (2025). Because river water typically freezes from about November to the following April, suspended sediment observations were conducted annually from May to October. The geospatial data used in Fig. 1a include topographic data obtained from the NASA Earthdata Search platform (https://search.earthdata.nasa.gov) and land use data, including glacier extent, obtained from National Tibetan Plateau/Third Pole Environment Data Center (http://data.tpdc.ac.cn). Meteorological data were obtained from LESMDON and in situ rain gauge measurements, while snow cover fraction was derived from MODIS remote sensing products accessed via the NASA National Snow and Ice Data Center (NSIDC) (https://nsidc.org/home).

https://doi.org/10.5194/egusphere-2026-4910
Preprint. Discussion started: 15 September 2026

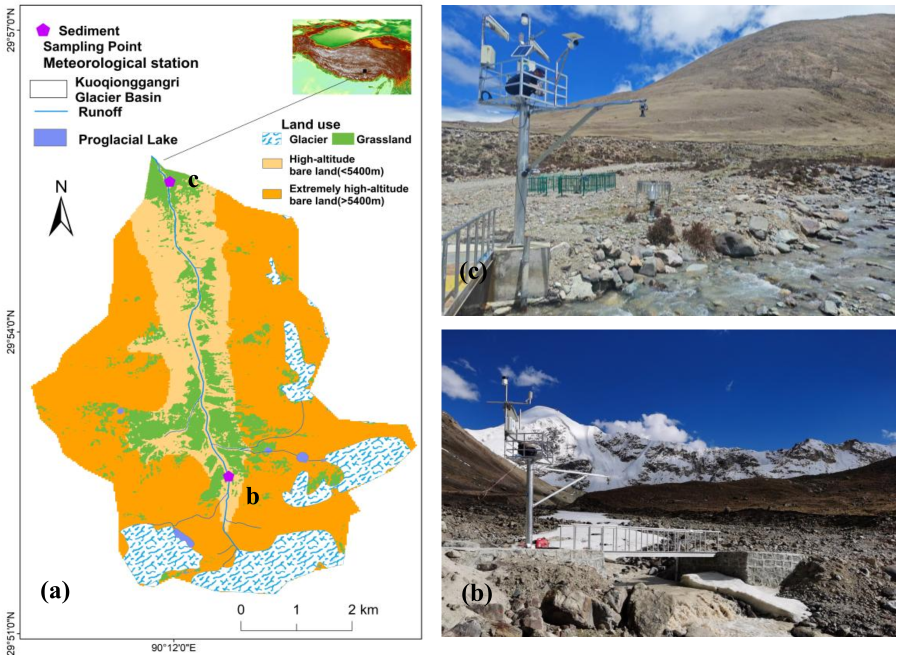

Fig. 1. Geographic location and land use types of the Kuoqionggangri Glacier Basin (a). (b) and (c) are close-up photographs of the glacier terminus and basin outlet cross-sections, respectively.

2.2 In situ Monitoring and Sampling

Continuous and automated monitoring of runoff turbidity was conducted using the turbidity sensors (OBS-3+, Campbell Scientific Inc., CSI) factory calibrated with a measurement range of 0 to 6000 NTU. Each sensor was housed in a perforated steel sleeve (20 cm in diameter and 2 m in length) and mounted beneath the pedestrian bridges at the two cross sections (Fig. 1). The sensors were positioned to remain continuously submerged, approximately 20 cm above the riverbed, and aligned parallel to the flow direction. Turbidity was recorded every 10 minutes as a continuous time series. Sensors were cleaned twice per year to remove fouling and debris that could otherwise compromise measurement accuracy.

Converting turbidity to SSC requires concurrent, intensified in situ sampling at both cross sections, namely the glacier terminus and the basin outlet. From 2021 to 2024, intensive sampling

https://doi.org/10.5194/egusphere-2026-4910
Preprint. Discussion started: 15 September 2026

was conducted at both sections to capture sediment dynamics during snowmelt-, glacier melt-, and rainfall-dominated periods. The criteria used to delineate these three periods on the basis of turbidity, air temperature, precipitation, and related observations are described in Liu et al. (2025), and field photographs of runoff conditions reveal pronounced differences in sediment characteristics among them (Fig. S1). Given the logistical constraints of fieldwork, sampling on non-rainfall days was generally undertaken when temperatures were relatively high and sediment changes were clearly visible, typically between 14:00 and 19:00. On rainfall days, sampling began at the onset of daytime precipitation and ended two hours after rainfall ceased; nocturnal rainfall events were not considered. To account for vertical variability, each 1 L sample comprised two 0.5 L subsamples collected at approximately one quarter and three quarters of the flow depth below the surface. Sampling intervals were set at 30 minutes under low-SSC conditions and 10 minutes under high-SSC conditions, yielding a total of 370 suspended sediment samples.

In addition, soil samples from potential sediment source areas were collected. The classification of potential source areas and the sampling strategy followed Liu et al. (2025). The dominant land cover types in the study area include glaciers, bare land (subdivided into extremely high-altitude and high-altitude bare land), and alpine meadow.

2.3 Sample treatment and measurement

Water samples were filtered immediately after collection through pre-combusted 1.2 μm Whatman GF/C glass-fibre filters for the determination of SSC, which was measured using the standard gravimetric framework. Specifically, the filters were oven-dried at 105 °C for at least 2 h to constant weight, and SSC was calculated from the difference in filter mass before and after filtration and drying divided by the volume of water filtered. Because of limitations in sampling frequency, the highest turbidity associated with field-collected suspended sediment samples was

https://doi.org/10.5194/egusphere-2026-4910
Preprint. Discussion started: 15 September 2026

obviously lower than the turbidity sensor recorded peak value.

In addition to SSC determination, both suspended sediment and source soil samples were analyzed for grain-size distribution and organic-matter content. Prior to analysis, samples were air-dried at room temperature, gently disaggregated, and passed through a 2 mm sieve to remove coarse debris. The <2 mm fraction was then further homogenized using an agate mortar and pestle to ensure representative subsampling. Grain size distribution was determined using a combination of dry sieving and laser diffraction. All samples were first fractionated by dry sieving through a nested series of standard meshes, and each size fraction was weighed to determine its mass percentage (Fig. S2). To further characterize the fine fractions and validate the sieve-derived results for particles finer than sand, selected representative samples were additionally analyzed using a laser particle size analyzer (Malvern Mastersizer 2000, UK). Prior to laser analysis, approximately 20 mL of H_2O_2 was added to remove organic matter, and the suspension was heated to near boiling. Subsequently, 3~4 drops of HCl were added to remove carbonates. After the reaction had proceeded to completion, the supernatant was decanted, and the treated sample was dispersed and measured using the laser analyzer (Callesen et al., 2018). The conversion relationship between sieve-based and laser-based grain-size results is provided in Text S1 in the Supplemental Material.

Organic-matter content was determined for the $\leq$ 2 mm fraction. After sieving and homogenization, samples were analyzed for organic carbon using a TOC-V analyzer. Where necessary, pretreatment was carried out to remove inorganic carbon prior to measurement, and the resulting organic carbon content was employed as a proxy for organic-matter content. Detailed procedures for the collection and processing of source soils from different land cover types are described in Liu et al. (2025).

https://doi.org/10.5194/egusphere-2026-4910
Preprint. Discussion started: 15 September 2026

2.4 Lab experiments

To elucidate the key factor driving variability in turbidity–SSC relationships and to develop an extended, high precision relationship that compensates for limitations in field sampling, a suite of controlled laboratory mixing experiments was designed and conducted. The experimental setup comprised a cylindrical tank with a diameter of 0.6 m, a mixer, a current meter, a turbidity sensor, and a supporting frame (Fig. S3). Sediment/soil materials were mixed with water at prescribed concentrations. Mixer speed was adjusted to reproduce the flow velocities observed during field monitoring, which were measured using the same current meter as in the field. During each run, the mixture was continuously stirred and turbidity was recorded in real time. Readings were taken at 1- minute intervals, and the mean of three consecutive measurements was used as the turbidity value for each run.

The mixing experiments comprised four sets of trials:

(1) Preliminary tests: Suspended sediments from the glacier terminus and basin outlet cross sections were used to reproduce field-measured turbidity–SSC relationships under different experimental conditions and to rigorously verify the experimental design;

(2) Group A: Mixtures with a range of SSCs were prepared from individual source materials, including glacier moraine material, extremely high-altitude bare-land soil, high-altitude bare-land soil, and meadow soil, to establish turbidity–SSC curves for materials with different particle sizes. Median grain size (D50) was used as the primary descriptor of particle size because suspended sediment derived from the same source material and comparable event types was relatively homogeneous, making a single summary metric appropriate for comparing particle-size effects among source materials (De Lange et al., 2024). Here, D50 denotes the grain size at which 50 % of the cumulative mass or volume distribution is finer;

https://doi.org/10.5194/egusphere-2026-4910
Preprint. Discussion started: 15 September 2026

(3) Group B: Suspensions from a single source were prepared with different organic matter contents to evaluate the effect of organic matter on turbidity–SSC relationships;

(4) Group C: The proportional composition of grain size fractions in suspended sediment samples from periods dominated by different hydrological processes was used to prepare a series of mixtures with varying SSCs. The resulting turbidity–SSC curves were used to reconstruct and extend field-derived turbidity–SSC relationships.

Other factors, such as flow velocity and particle color, have been shown in previous studies to exert only minor effects on turbidity–SSC relationships under comparable conditions (e.g., Sehgal et al., 2022). In addition, because clay sized particles (<50 μm) can flocculate in water and form larger aggregates (Soulsby et al., 2001; Woźniak et al., 2010; Kostaschuk et al., 2018; Merten et al., 2014; Felix et al., 2018; Druine et al., 2018; Sehgal et al., 2022), size classes finer than 50 μm were not further subdivided in the experiments. The detailed experimental design is provided in Table 1.

2.5 data analysis

Field sampled and measured SSCs were paired with the corresponding turbidity observations, and their relationship was modelled using a power law function ($y = ax^b$). Unlike the linear regressions commonly used in previous studies (Sehgal et al., 2022), a power law formulation was adopted, consistent with the hysteresis relationship between turbidity and SSC reported by Landers et al. (2013).

https://doi.org/10.5194/egusphere-2026-4910
Preprint. Discussion started: 15 September 2026

Table 1. Experimental design for the laboratory mixing trials of turbidity–SSC relationships.

Experiment	Objective	Trial Group Names	Trial Counts	Sediment Composition	Key Experimental Variables
Preliminary Experiment	Verify the feasibility of the experiment design	Pre E1	100	Suspended Sediment Collected from the Glacier Terminus	SSC: 0.03~15.00 kg/m^3
		Pre E2	300	Suspended Sediment Collected from the basin Outlet	SSC: 0.02~9.00 kg/m^3
Group A Experiment	Establish turbidity–SSC relationship curves to analyze the influence of particle size	Group A1	50	Moraine Material	Median Particle Size (D_{50}): 31.45 μm
		Group A2	50	Extremely High-Altitude Bare Soil	Median Particle Size (D_{50}): 24.00 μm
		Group A3	50	High-Altitude Bare Soil	Median Particle Size (D_{50}): 19.21 μm
		Group A4	50	Meadow Soil	Median Particle Size (D_{50}): 4.62 μm
Group B Experiment	Establish turbidity–SSC relationship curves to analyze the influence of organic matter content	Group B1	50	Moraine Material	SOC: 0.01%~0.13%
		Group B2	50	Extremely High-Altitude Bare Soil	SOC: 0.14%~0.31%
		Group B3	50	High-Altitude Bare Soil	SOC: 0.36%~0.56%
		Group B4	50	Meadow Soil	SOC: 1.27%~2.81%
Group C Experiment	Reproduce and extend turbidity–SSC relationships	Group C1	1056	Snowmelt Period Suspended Sediment from the Glacier Terminus	Grain Size:⩽1250 μm
		Group C2	635	Glacier Melt Period Suspended Sediment from the Glacier Terminus	Grain Size: ⩽2000 μm
		Group C3	465	Rainfall Period Suspended Sediment from the Glacier Terminus	Grain Size:⩽900 μm
		Group C4	1106	Snowmelt Period Suspended Sediment from the Basin Outlet	Grain Size:⩽600 μm
		Group C5	882	Glacier Melt Period Suspended Sediment from the Basin Outlet	Grain Size:⩽900 μm
		Group C6	1358	Rainfall period Suspended Sediment from the Basin Outlet	Grain Size:⩽350 μm

https://doi.org/10.5194/egusphere-2026-4910
Preprint. Discussion started: 15 September 2026

The power-law relationship is empirical, and its fitted coefficients do not have direct physical meanings. However, variations in *a* and *b* can be interpreted in relation to sediment supply, particle characteristics, and the transport capacity of flowing water. In this respect, the turbidity–SSC relationship is analogous to conventional sediment–water relationships, such as discharge–sediment load relationships, in which empirical parameters reflect the combined effects of sediment availability and hydraulic forcing (Walling, 1977). To improve SSC estimation at each cross-section, separate turbidity–SSC relationships were developed for periods dominated by snowmelt, glacier melt, and rainfall. Model performance was evaluated using the correlation coefficient (R^2), the Nash–Sutcliffe efficiency (NSE) coefficient, and root mean square error (RMSE). The definitions of these metrics are provided in Text S2 in the Supplemental Material.

3 Result

3.1 Variation of turbidity at the glacier terminus and basin outlet

Turbidity monitoring results for the glacier terminus and basin outlet sections of the Kuoqionggangri Glacier Basin from 2021 to 2024 are shown in Fig. S4, marked with periods dominated by snowmelt, glacier melt, and rainfall determined following Liu et al. (2025). The records reveal pronounced contrasts in turbidity dynamics between the two sections. At the glacier terminus, intense fluctuations were concentrated mainly from May to August, reflecting the strong influence of glacier melt and snowmelt (Fig. S4). During this period, meltwater delivered large volumes of sediment to the channel at the glacier terminus, producing markedly elevated turbidity. About 4.8% of observations exceeded 500 NTU, with multiple exceptionally high peaks; maxima reached 4633 NTU during the glacier melt period and 3330 NTU during the snowmelt period. These peaks were typically associated with intense rapid glacier ablation or snowmelt episodes, indicating that temperature driven meltwater pulses can trigger severe erosion and sediment transport above the glacier terminus, thereby increasing SSCs and, in turn, turbidity. By contrast, in September and October, when glacier melt and snowmelt no longer dominated, turbidity remained relatively low; only 0.2% of observations exceeded 500 NTU, indicating substantially weaker erosion and sediment export at the glacier terminus during this period.

Compared with the glacier terminus, turbidity at the basin outlet exhibits a much more pronounced seasonal variation (Fig. S4). Peaks are higher, reaching a maximum of 5476 NTU, and occur mainly during the summer glacier melt and rainfall dominated periods (July to August), with rainfall driven erosion being concentrated in the middle and lower parts of the basin. During the spring snowmelt period, turbidity at the basin outlet is markedly lower than at the glacier terminus, with a maximum of 2421 NTU. This likely reflects the fact that sediment during this period is sourced primarily from the glacier terminus and is subsequently deposited during river channel transport, substantially dampening turbidity peaks at the outlet. By contrast, during the glacier melt and rainfall dominated periods, turbidity variability at the basin outlet is more pronounced than at the glacier terminus. This is particularly evident during the rainfall period, when turbidity peaks at 5477 NTU, and such high values are closely associated with relatively intense rainfall events, a pattern that differs from the dynamics at the glacier terminus. Moreover, during the snowmelt and glacier melt periods, the overall turbidity trajectory at the basin outlet broadly mirrors that at the glacier terminus, yet diurnal peak timings are slightly delayed by about 1 to 2 h, consistent with the sediment travel time from the glacier terminus to the basin outlet.

3.2 Field-derived turbidity–SSC relationships

Fig. 2(a) shows the field-derived turbidity (y)–SSC (x) relationships at the glacier terminus and basin outlet when all observations were pooled without accounting for hydrological period differences. Clear differences were observed between the two cross-sections. At the glacier

https://doi.org/10.5194/egusphere-2026-4910
Preprint. Discussion started: 15 September 2026

terminus, the fitted relationship is $y = 0.0012x^{1.26}$ ($R^2 = 0.85$), whereas at the basin outlet it is $y = 0.0008x^{1.22}$ ($R^2 = 0.86$). Both parameters are higher at the glacier terminus, particularly the exponent, indicating a steeper scaling in which SSC responds more sharply to changes in turbidity at the glacier terminus than at the basin outlet. Notably, however, regressions fitted without accounting for additional controls show only moderate accuracy.

Recognizing that sediment sources are broadly comparable within periods dominated by a single hydrological driver (Liu et al., 2025), the turbidity–SSC data were divided by the dominant hydrological regime (e.g., snowmelt, glacier melt, and rainfall). Fig. 2(b) presents the regression results for both sections across the three periods. After this stratification, the goodness of fit (R^2) of the power law regressions improves markedly, and clear differences emerge among the regimes. For example, at the glacier terminus, the fitted relationships are $y = 0.0021x^{1.15}$ ($R^2 = 0.98$) during the snowmelt period, $y = 0.0032x^{1.18}$ ($R^2 = 0.92$) during the glacier melt period, and $y = 0.0017x^{1.12}$ ($R^2 = 0.78$) during the rainfall-dominated period. At the basin outlet, the fitted relationships are $y = 0.0007x^{1.29}$ ($R^2 = 0.96$) during the snowmelt period, $y = 0.0024x^{1.07}$ ($R^2 = 0.94$) during the glacier melt period, and $y = 0.0007x^{1.16}$ ($R^2 = 0.93$) during the rainfall-dominated period. These results indicate that process-based stratification better captures the variability in turbidity–SSC relationships under contrasting runoff and sediment-supply conditions.

https://doi.org/10.5194/egusphere-2026-4910
Preprint. Discussion started: 15 September 2026

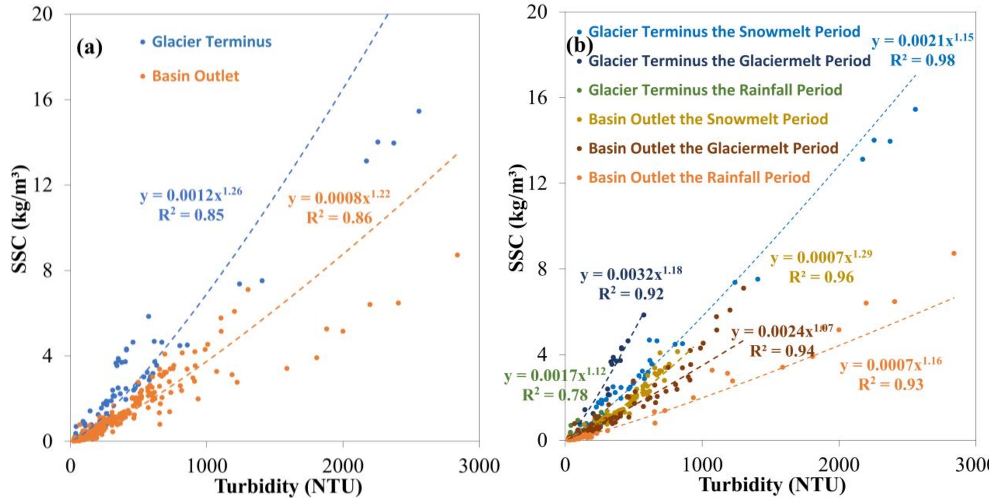

Fig. 2. (a) Field-observed turbidity–SSC relationship; (b) fitted turbidity–SSC relationships for the three periods at the two cross-sections.

It should be noted that the maximum turbidity paired with field measured SSCs was 2840 NTU, whereas the turbidity sensor recorded a peak value of 5580 NTU. This mismatch mainly reflects the short-lived nature of extreme turbidity peaks, which are difficult to capture through manual sampling under field conditions. Consequently, the effective calibration range of the field-derived turbidity–SSC relationships is limited. Although the period specific regressions markedly improve goodness of fit, it remains unclear whether the fitted functions can be extrapolated reliably to estimate SSCs at high turbidity (>2840 NTU). Such extrapolation would still carry substantial uncertainty that is inherent to the dataset because observations increasingly deviate from the fitted curves as turbidity increases. To illustrate this limitation, two cases spanning relatively wide turbidity ranges were selected: the glacier terminus during the snowmelt period and the basin outlet during the rainfall period. For each case, the dataset was divided into two subsets. Observations with turbidity <1400 NTU were first used to fit a turbidity–SSC relationship, which was then extrapolated to estimate SSC in the medium-turbidity range of 1400~3000 NTU. Measured SSCs within this medium turbidity range were used for validation, and predictive

https://doi.org/10.5194/egusphere-2026-4910
Preprint. Discussion started: 15 September 2026

performance was evaluated using the Nash–Sutcliffe efficiency (NSE) and root mean square error (RMSE).

The results show that, although the fitted turbidity–SSC curves perform well within the observed range of turbidity <1400 NTU, extrapolating them to 1400~3000 NTU yields very poor accuracy and introduces substantial uncertainty (Fig. 3). For the glacier terminus during snowmelt, the regression fitted to turbidity <1400 NTU is $y = 0.0018x^{1.18}$ (RMSE = 0.70 kg/m^3), but when extrapolated to 1400~3000 NTU and validated against observations, performance declines to NSE = 0.11 and RMSE = 2.59 kg/m^3. For the basin outlet during rainfall, the regression fitted to turbidity <1400 NTU is $y = 0.0008x^{1.10}$ (RMSE = 0.53 kg/m^3), yet extrapolation to 1400~3000 NTU yields NSE = −0.67 and RMSE = 2.14 kg/m^3 against measured values. These results indicate that the low- and medium-turbidity ranges are not governed by a single invariant relationship. Therefore, a curve fitted to lower turbidity values cannot reliably convert higher turbidity observations into SSC, particularly when high-end observations are sparse. The fixed regression form fails to capture the systematic evolution of the turbidity–SSC relationship across the full turbidity range. This limitation motivates the need for a framework that can extend turbidity–SSC relationships when field sampling provides only limited coverage of high-turbidity conditions.

https://doi.org/10.5194/egusphere-2026-4910
Preprint. Discussion started: 15 September 2026

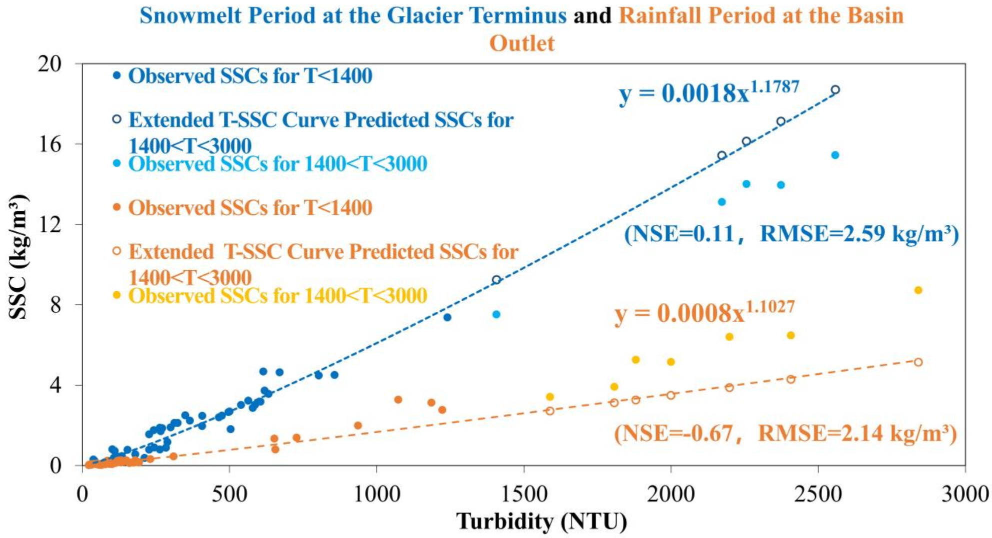

Fig. 3. Validation of extrapolated turbidity–SSC relationships for the snowmelt period at the glacier terminus section and the rainfall-dominated period at the basin-outlet section.

3.3 Reproducing field derived turbidity–SSC relationships and identifying their primary controls in the lab

The preliminary laboratory mixing experiments successfully reproduced the field derived turbidity–SSC relationship, confirming the suitability of the experimental framework (Fig. S5). Comparison of turbidity values at equivalent SSCs showed strong agreement between the laboratory trials and field observations, with NSE = 0.96 and RMSE = 7.07 NTU. The fitted power law parameters were likewise highly consistent between the laboratory and field datasets (Table S1). These results indicate that the mixing experiments can reproduce the main turbidity–SSC relationship observed under natural runoff-driven suspended-sediment transport conditions.

The mechanisms driving differences in turbidity–SSC relationships were then examined. Group A experiments established turbidity–SSC relationships for single source soils with contrasting gain sizes to evaluate the influence of grain size distributions (Fig. S6). Consistent with Landers et al. (2013), the results show that turbidity–SSC relationships in this high-altitude

https://doi.org/10.5194/egusphere-2026-4910
Preprint. Discussion started: 15 September 2026

glacier basin are strongly controlled by particle size. The curves derived from mixtures of different source soil, including glacier moraine material, extremely high-altitude bare land soil, high-altitude bare land soil, and meadow soil, differed markedly from one another, whereas each fitted curve showed very high goodness of fit, with R^2 close to 1. This indicates strong within source consistency and clear between source contrasts. Across source materials, coarser mixtures, such as those derived from glacier moraine material, produced substantially higher SSCs than finer mixtures, such as those derived from meadow soil, at a given turbidity. This pattern occurs because finer particles scatter light more efficiently and therefore generates higher turbidity readings at the same mass concentration (Gray and Gartner, 2009).

Organic matter content may also influence turbidity–SSC relationships. In the study basin, however, organic matter content varies only modestly among source materials: meadow soils were comparatively enriched (2.81%), whereas all other soil types contain <1%. Group B experiments were therefore used to assess the effect of organic matter by establishing turbidity–SSC relationships for materials with similar grain-size ranges but different organic-matter contents. The fitted curves under contrasting organic matter levels were broadly similar, likely because organic matter contents were generally low and varied within a narrow range (Fig. S7). Overall, differences in organic-matter content exerted only a minor influence on turbidity–SSC relationships in this basin, and their effect was substantially weaker than that of grain size.

3.4 Reproducing and extending turbidity–SSC relationships based on grain-size composition

The results in Sect. 3.3 highlight the dominant role of grain size in controlling turbidity–SSC relationships and provide the basis for the Group C experiments. This study therefore infer that variations in suspended sediment grain-size composition under contrasting hydrological conditions are a primary driver of the observed variability in turbidity–SSC relationships.

https://doi.org/10.5194/egusphere-2026-4910
Preprint. Discussion started: 15 September 2026

Fig. S8 shows the grain-size distributions of suspended sediment collected at the Kuoqionggangri glacier terminus and basin outlet during the snowmelt-, glacier melt-, and rainfall-dominated periods. The results reveal pronounced differences in grain-size composition among periods and between cross-sections. These contrasts reflect shifts in hydro-meteorological conditions and sediment source zones within the basin, which in turn modify the turbidity–SSC relationship.

Further classification by grain-size fraction showed that suspended sediment samples from the same cross-section and hydrological period had broadly similar grain-size compositions, while the proportion of each fraction varied systematically with turbidity (Fig. S9). Quantitative relationships between turbidity and the proportional composition of suspended sediment grain-size fractions were therefore established for the three hydrological periods at both cross-sections (Fig. S10). The percentage contribution of each size fraction showed a relatively stable increasing or decreasing trend with increasing turbidity. Overall, finer fractions decreased progressively, whereas coarser fractions increased, likely reflecting changes in flow hydraulics and sediment transport capacity. Except during the glacier melt and rainfall periods at the glacier terminus, most cases covered a relatively wide turbidity range. For periods spanning a wide turbidity range, the low-turbidity range (<200 NTU) was excluded from the subsequent extension because it corresponded to low SSCs and exhibited limited variation in grain-size composition; within this range, the 0.5–50 μm fraction generally accounted for at least 95 % of the suspended material. These results indicate that differences in turbidity–SSC relationships among periods and cross-sections are closely linked to the evolving grain-size composition of suspended sediment. The snowmelt period at the glacier terminus is used here as an illustrative example, with the complete results provided in the Supplement.

https://doi.org/10.5194/egusphere-2026-4910
Preprint. Discussion started: 15 September 2026

During the snowmelt period at the glacier terminus (Fig. S9), the proportion of the 0.5–50 μm fraction decreased with increasing turbidity, from 87.5% at 226 NTU to 76.9% at 1240 NTU. By contrast, the proportions of the 50–75 μm, 75–125 μm, 125–250 μm, 250–320 μm, 320–500 μm, 500–900 μm, and 900–1250 μm fractions increased gradually. Similar turbidity–grain-size proportion relationships were observed for the other periods and cross-sections, although the upper grain-size limit differed among cases. The nonlinear evolution of grain-size proportions with increasing turbidity reflects the combined effects of changing hydraulic conditions and particle settling behavior.

The feasibility of extrapolating grain-size composition proportion to higher turbidity was then evaluated. For the snowmelt period at the glacier terminus, the dataset was divided into a low-turbidity fitting segment (<1400 NTU) and a medium-turbidity validation segment (1400–3000 NTU; Fig. 4). Each grain-size fraction was fitted as a function of turbidity using a power-law relationship. In Fig. 4a, the solid curves represent the fitted relationships in the low-turbidity segment, whereas the dashed curves represent their extrapolation into the validation segment. For each turbidity value in the validation segment, the corresponding value on the dashed curve gives the extrapolated percentage contribution of a given grain-size fraction, which was then compared with the measured value.

The set of fitted power-law functions for the different grain-size fractions ($p_i(T)$), where (i) denotes the grain-size class and (T) denotes turbidity, must satisfy the mass-balance constraint:

$$\sum_{i=1}^{n} p_i(T) = 100\% \qquad (1)$$

where $p_i(T)$ is the fitted percentage contribution of the i-th grain-size fraction. Thus, for each turbidity level, the sum of the fitted proportions across all grain-size fractions must equal 100 %. To satisfy this constraint, one fraction was defined as the residual term:

https://doi.org/10.5194/egusphere-2026-4910
Preprint. Discussion started: 15 September 2026

$$p_n(T) = 100\% - \sum_{i=1}^{n-1} p_i(T) \quad (2)$$

This residual formulation ensures that the extrapolated grain-size composition remains physically consistent at each turbidity level.

Using the turbidity–grain-size relationships derived from the low-turbidity fitting segment for the snowmelt period at the glacier terminus (Text S3), grain-size composition was extrapolated into the validation segment and evaluated against measured values. The extrapolated grain-size composition agreed well with the observations, with NSE = 0.91. Overall, increasing turbidity was accompanied by a progressive decrease in the proportion of finer suspended particles, such as the <75 μm fractions, and a corresponding increase in coarser fractions, such as the 125–250 μm fraction. This systematic pattern indicates that turbidity–grain-size composition relationships calibrated in the lower turbidity range can be reasonably extrapolated to medium-turbidity conditions.

https://doi.org/10.5194/egusphere-2026-4910
Preprint. Discussion started: 15 September 2026

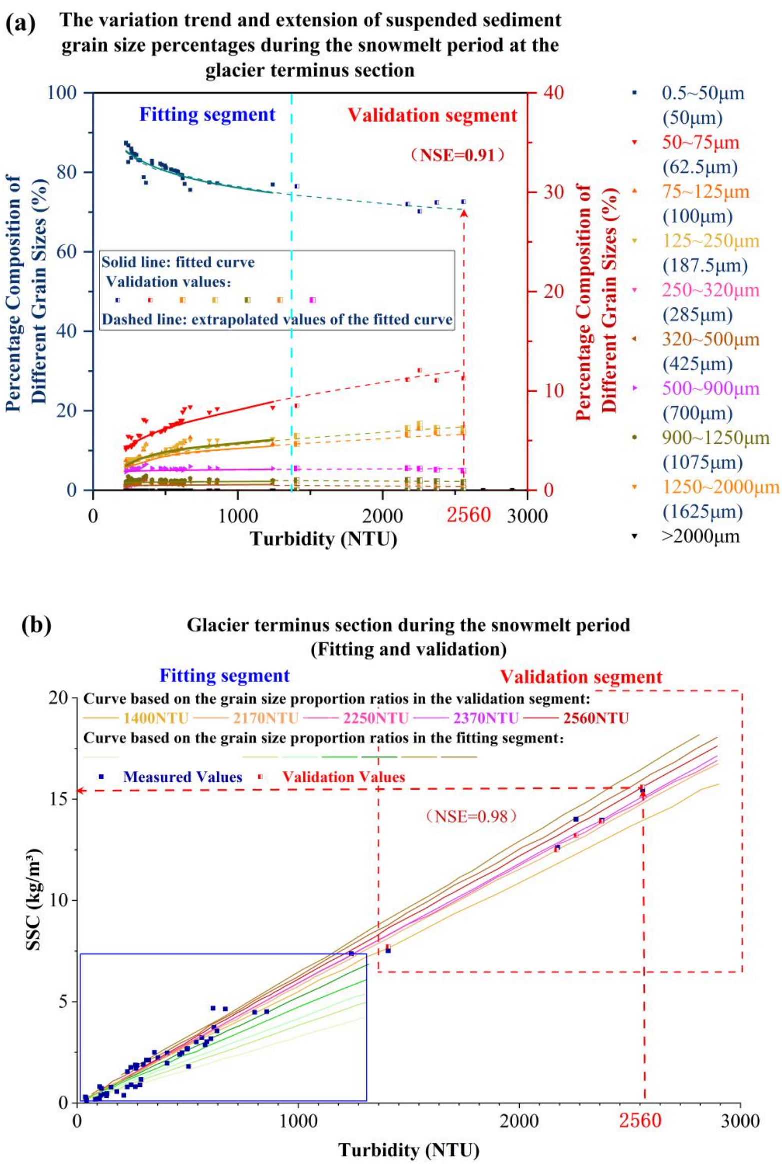

Fig. 4. Validation procedure for (a) extending suspended sediment grain-size composition proportion, and (b) expanding the turbidity–SSC relationship through particle size percentages (a) proportioning tests (The proportioning test results of the fitting section are shown in the blue box, more groups of tests were conducted to ensure the feasibility).

The next step was to test whether SSC in the validation segment could be accurately derived

https://doi.org/10.5194/egusphere-2026-4910
Preprint. Discussion started: 15 September 2026

from the extrapolated grain-size composition. Group C experiments were therefore conducted to generate turbidity–SSC curves for the extrapolated grain-size compositions corresponding to different turbidity levels. For each target turbidity, the corresponding grain-size composition was first obtained from the extrapolated turbidity–grain-size relationships shown in Fig. 4a. A sediment mixture with this grain-size composition was then prepared, and a series of suspensions with increasing SSCs was produced to establish the corresponding laboratory-derived turbidity–SSC curve. The SSC associated with the target turbidity was then determined from this curve. By repeating this procedure for each target turbidity, a series of turbidity–SSC curves were generated and the corresponding SSC estimates were obtained.

For example, for a turbidity of 2560 NTU, the corresponding grain-size composition was first derived from the extrapolated turbidity–grain-size relationships in Fig. 4a. The laboratory-derived turbidity–SSC curve for this grain-size composition was then used to determine SSC, as illustrated in Fig. 4b. SSC estimates obtained using this procedure agreed closely with observations in the validation range, with NSE = 0.98 and RMSE = 0.85 kg/m^3. This performance was substantially better than that obtained by direct extrapolation of the turbidity–SSC relationship, which yielded NSE = 0.11 and RMSE = 2.59 kg/m^3). Similar results were obtained for the other cross-sections and hydrological periods (Figs. S10 and S11), with NSE values of 0.96–0.98 and RMSE values of 0.85–0.93 kg/m^3. These results demonstrate that the proposed grain-size-informed framework can extend turbidity–SSC relationships beyond the range constrained by paired field samples.

The framework was then applied to derive SSCs at higher turbidity levels. For each hydrological period and cross-section, power-law relationships between turbidity and grain-size composition were fitted over the available field-sampling range and then extrapolated to higher turbidity levels (Fig. S12). The fitting ranges were <3000 NTU for the snowmelt period at the

https://doi.org/10.5194/egusphere-2026-4910
Preprint. Discussion started: 15 September 2026

glacier terminus, <600 NTU for the glacier melt period at the glacier terminus, <300 NTU for the rainfall period at the glacier terminus, <1000 NTU for the snowmelt period at the basin outlet, <1500 NTU for the glacier melt period at the basin outlet, and <3000 NTU for the rainfall period at the basin outlet. The fitted turbidity–grain-size relationships performed well, with NSE values of 0.91~0.96. Following the same procedure used for the validation range, laboratory mixtures were prepared using the extrapolated grain-size compositions associated with higher turbidity levels, and the resulting turbidity–SSC curves were used to derive SSCs for the extended turbidity range (Fig. S13).

In summary, extrapolation of suspended sediment grain-size composition, coupled with laboratory mixing experiments, enabled turbidity–SSC conversion relationships to be established for the high turbidity domain across all three hydrological periods at both the glacier terminus and basin outlet (Fig. 5). Across the two cross-sections and dominant hydrological regimes, the extended relationships covered maximum turbidity values of approximately 2000~6000 NTU. Differences in these maxima mainly reflect variations in the proportional increase of coarser suspended material (≥75 μm) among cases. A greater increase in the ≥75 μm fraction leads to a higher SSC at a given turbidity, thereby altering the upper range over which the turbidity–SSC relationship can be extended.

https://doi.org/10.5194/egusphere-2026-4910
Preprint. Discussion started: 15 September 2026

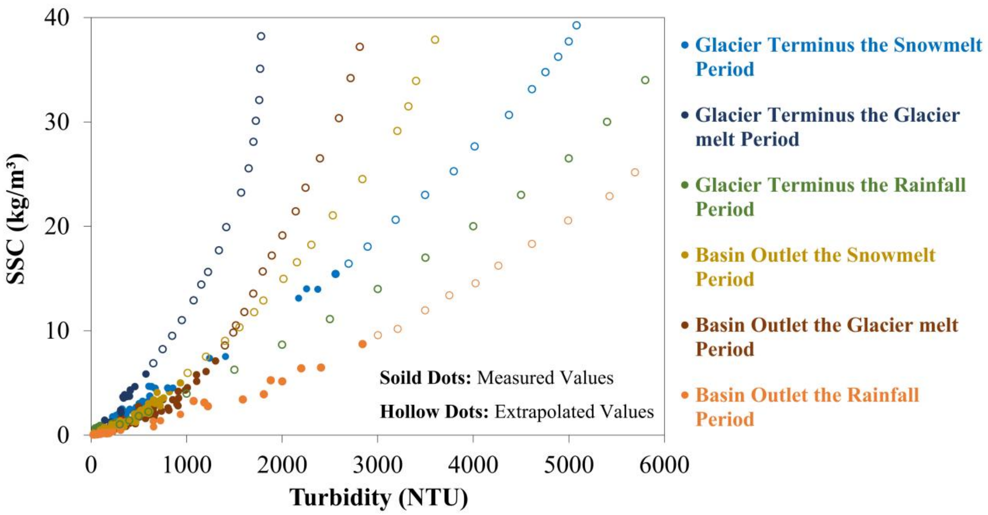

Fig. 5. Extended turbidity–SSC relationships for the three periods at the two sections in the Kuoqionggangri Glacier Basin.

4 Discussion

4.1 Grain-size distribution controls on turbidity–SSC relationships

Field turbidity monitoring, sediment sampling, grain-size analysis, and controlled laboratory mixing experiments at the glacier terminus and basin outlet provide a basis for examining suspended sediment transport in glacier basins and its controlling factors. The results show that turbidity, and therefore SSC, at both cross-sections is strongly influenced by contrasting erosion and transport processes associated with snowmelt, glacier melt, and rainfall. The turbidity–SSC relationship was not constant across these hydrological periods, mainly because of systematic differences in suspended-sediment grain-size distributions. This finding is broadly consistent with the relationships among concentration, turbidity, and discharge reported by Landers et al. (2013). Accordingly, partitioning the data by hydrological period substantially improved the fit of the turbidity–SSC relationships. The fitted curves show that, within a given period, the relationship at the glacier terminus was generally steeper than that at the basin outlet, whereas the rainfall period

https://doi.org/10.5194/egusphere-2026-4910
Preprint. Discussion started: 15 September 2026

produced the gentlest relationship at both cross-sections. Comparisons of suspended sediment samples among periods and cross-sections suggest that these patterns reflect differences in sediment properties generated by contrasting erosion and transport processes.

Consistent with previous studies, the results indicate that turbidity–SSC relationships are controlled primarily by suspended sediment grain-size distribution, whereas organic matter content plays a secondary role, partly through its influence on particle density and settling velocity (Mager and Horton, 2025). By contrast, factors such as flow velocity and particle color appear to exert only minor effects on turbidity–SSC relationships under comparable conditions (Kim et al., 2025). These findings are consistent with the general relationship among turbidity, grain size, and organic matter content proposed by Sehgal et al. (2022), although both turbidity and SSC were substantially higher in the present glacier basin than in their study. Physically, fine particles, such as clay and silt, remain in suspension longer and scatter light more efficiently than coarser sand sized particles, thereby contributing disproportionately to turbidity at a given mass concentration. These results support the use of grain-size distribution as the main basis for interpreting turbidity–SSC variability in the glacier basin.

Field-measured suspended-sediment grain-size distributions were therefore incorporated into the analysis of turbidity–SSC relationships. Grain-size measurements show marked differences in both the range and shape of the distributions among hydrological periods and between cross-sections. At the glacier terminus, maximum grain sizes during the snowmelt, glacier melt, and rainfall periods were 1250 µm, >2000 µm, and 900 µm, respectively, whereas the corresponding maxima at the basin outlet were 600, 900, and 350 µm. These differences indicate that coarse particles were transported more readily near the glacier terminus, whereas downstream transport involved selective settling and progressive fining. Pfannkuche and Schmidt (2003) showed that

https://doi.org/10.5194/egusphere-2026-4910
Preprint. Discussion started: 15 September 2026

turbidity–SSC relationships may diverge with increasing runoff because of changes in sediment grain-size distribution. To describe these contrasts more fully, the particle size spectrum was divided into ten fractions spanning the observed range. The results show that, within a given cross section and hydrological period, grain-size distributions shifted systematically with increasing turbidity, providing the basis for laboratory mixing experiments used to validate and extend the corresponding turbidity–SSC relationships.

Across the three hydrological periods, the glacier terminus generally contained a higher proportion of coarse suspended particles than the basin outlet, indicating a stronger glacier derived sediment signal. During the snowmelt period, the proportion of particles <50 µm was lower at the glacier terminus than at the basin outlet, whereas the 50~500 µm fraction was broadly comparable between the two cross-sections. A minor 900~1250 µm fraction occurred only at the glacier terminus, accounting for approximately 0.5 % of the total and showing little variation with increasing turbidity; this fraction was absent at the basin outlet. These differences help explain why the turbidity–SSC curve at the glacier terminus was slightly steeper. However, because the 50~500 µm fraction increased more strongly with turbidity at the basin outlet, the slopes of the two curves progressively converged. The extrapolated trends further suggest that the basin outlet curve could eventually exceed that of the glacier terminus. This pattern likely reflects enhanced hillslope snowmelt runoff and the associated increase in flow energy. The progressive coarsening of suspended sediment at the basin outlet with increasing turbidity therefore helps explain the observed change in the turbidity–SSC relationship.

During the glacier melt period, the tendency for suspended sediment to become progressively coarser with increasing turbidity was especially pronounced, and the contrast between the two cross-sections became more marked. At a given turbidity, the proportion of particles <50 µm was

https://doi.org/10.5194/egusphere-2026-4910
Preprint. Discussion started: 15 September 2026

markedly lower at the glacier terminus, whereas particles >2000 µm were observed only at this cross-section, reflecting the abundant supply of coarse moraine derived sediment from the glacial zone. Correspondingly, the turbidity–SSC relationship at the glacier terminus was both the highest and the steepest, whereas that at the basin outlet was distinctly lower. This downstream reduction reflects selective settling during transport and mixing with sediment from multiple sources, both of which reduced the proportion of coarse suspended material.

During the rainfall period, both cross sections showed comparatively gentle turbidity–SSC relationships. The basin outlet was strongly dominated by fine particles, with the <50 µm fraction accounting for approximately 90 % of the total, indicating increased sediment contributions from non-glacier areas. By contrast, a small but increasing proportion of coarser particles in the 250~1250 µm range persisted at the glacier terminus, explaining why the turbidity–SSC relationship at this cross-section remained slightly higher than that at the basin outlet. From a hydrodynamic perspective, the persistence of these coarser particles during the rainfall period may be related to precipitation falling directly on the glacier surface. Rainfall can enhance runoff generation and glacier ablation through heat input, producing runoff that mixes rainfall with glacier meltwater. Where precipitation includes snowfall, subsequent melt can further contribute snowmelt to the runoff mixture. In both cases, small amounts of moraine material can be entrained, increasing the grain size of suspended sediment at the glacier terminus.

Comparisons among hydrological periods within the same cross section further support the link between grain-size composition and turbidity–SSC relationships. At the glacier terminus, the glacier melt period exhibited the coarsest suspended sediment and the highest turbidity–SSC curve, indicating the greatest transport capacity under intense meltwater supply and direct delivery of moraine material from the glacial zone. The snowmelt period was intermediate in both grain size

https://doi.org/10.5194/egusphere-2026-4910
Preprint. Discussion started: 15 September 2026

and curve position, reflecting continued glacier influence but weaker transport capacity than during peak glacier melt. The rainfall period contained the finest suspended material and showed the lowest and gentlest turbidity–SSC relationship at this cross section, suggesting that locally generated rainfall runoff was less effective at entraining coarse glacier derived sediment. A similar but weaker ordering was observed at the basin outlet. There, the glacier melt and snowmelt periods exhibited broadly similar grain-size distributions and turbidity–SSC curves within the low-turbidity range, whereas the rainfall period was characterized by the finest material and the lowest curve. These inter-period differences indicate that changes in sediment source are fundamental to the observed variability: the glacial zone dominated the supply of coarse sediment during snowmelt and especially glacier melt, whereas rainfall mobilized a larger proportion of fine material from bare land and meadow areas, particularly at the basin outlet.

Overall, reconstructing and extending the evolution of suspended sediment grain-size composition enabled field-derived turbidity–SSC relationships to be reproduced and extended with high accuracy. This capability is important for estimating SSC during extreme sediment transport events that are difficult to capture through field sampling.

4.2 Comparison with previous turbidity–SSC studies

The framework proposed in this study combines field-measured suspended sediment grain-size composition with controlled laboratory mixing experiments to construct, validate, and extend turbidity–SSC relationships. It therefore provides a complementary framework for estimating SSC from turbidity records in high altitude, cold region glacier basins. This is particularly important because routine field sampling is difficult in such environments, especially during short-lived extreme events. As a result, paired turbidity–SSC samples often fail to cover the upper end of the monitored turbidity range, and direct extrapolation of fitted relationships can introduce substantial

https://doi.org/10.5194/egusphere-2026-4910
Preprint. Discussion started: 15 September 2026

error, as shown here by NSE values ranging from -0.67 to 0.11.

Previous studies have also highlighted the importance of grain-size variability in turbidity–based SSC estimation. Felix et al. (2018) attributed mean relative errors of <20 % in turbidity–derived SSC estimates partly to temporal shifts in grain-size distribution, supporting the need to characterize grain-size evolution when constructing turbidity–SSC relationships. Our emphasis on grain-size composition is also consistent with the generalized framework of Sehgal et al. (2022), in which SSC is estimated from turbidity together with grain-size and organic matter variables. However, representing the entire grain-size distribution using a single median grain size may overlook important compositional changes. Similarly, Kim et al. (2025) controlled grain-size distributions in laboratory mixing experiments and showed that turbidity–SSC relationships are approximately linear when grain-size distribution is held constant. Their results, like ours, emphasize the need to account for compositional variability, although their study focused mainly on laboratory conditions and did not explicitly incorporate the in-situ evolution of suspended sediment grain-size composition.

Compared with these studies, the present framework directly links systematic, turbidity-dependent changes in suspended sediment grain-size composition to changes in turbidity–SSC relationships. The laboratory derived relationships were first validated against field observations and then used to extend field derived turbidity–SSC relationships beyond the range constrained by paired samples. This framework addresses the challenge posed by hydrodynamically driven changes in suspended sediment properties and provides a practical solution for glacier basins where sediment sources are diverse, hydrological conditions are complex, and extreme event samples are difficult to obtain.

4.3 Applicability and uncertainty of the proposed framework

https://doi.org/10.5194/egusphere-2026-4910
Preprint. Discussion started: 15 September 2026

The proposed framework achieved NSE values of 0.96~0.98 when validated against observations. By explicitly accounting for the temporal evolution of suspended sediment grain-size distributions and combining this information with controlled laboratory mixing experiments, the framework is well suited to multi-source water and sediment supply systems, such as glacier basins, where grain size composition varies substantially among hydrological periods and hydraulic conditions. These results demonstrate that incorporating field derived grain-size information can improve SSC estimation from turbidity records. However, because the framework relies on grain-size data, its application to other basins requires careful characterization of how suspended sediment grain-size distributions vary with seasonality, runoff source, and event type. This requirement is particularly important where rainfall–runoff–erosion processes are highly variable or scale dependent. For example, transient changes in discharge and turbidity sensitivity to rainfall forcing may become more difficult to interpret at larger spatial scales, where complex rainfall–runoff–erosion interactions can obscure event-scale relationships (Göransson et al., 2013).

The construction and extension of turbidity–SSC relationships through combined field monitoring and laboratory mixing experiments also take advantage of two important characteristics of the study basin: pronounced spatial contrasts in sediment grain size and generally low organic matter content. Because suspended sediment transport is mainly controlled by snowmelt, glacier melt, and rainfall, sediment sources tend to remain relatively consistent within each hydrological period. In other basins where suspended sediment contains higher or more variable organic matter contents, organic matter should be explicitly incorporated into turbidity–SSC calibration. Low density organic material can produce relatively high turbidity even at low SSCs (Downing, 2006), and neglecting this effect may bias SSC estimates (Voichick et al., 2018).

Additional environmental controls may further affect turbidity–SSC relationships. For

https://doi.org/10.5194/egusphere-2026-4910
Preprint. Discussion started: 15 September 2026

example, water temperature can influence flocculation and aggregation, thereby altering the optical properties of suspended particles, while pH can affect particle surface charge and aggregation behavior. These factors were not explicitly considered in the present framework and should be examined in future applications. Some uncertainty is also unavoidable despite efforts to minimize experimental error. The main sources include inaccuracies during laboratory sieving and weighing, deviations between fitted grain-size proportion curves and true grain-size compositions, and errors introduced when preparing laboratory mixtures from extrapolated grain-size proportions, including weighing and stirring inconsistencies.

5 Conclusion

This study developed and validated a grain-size informed framework that integrates in situ turbidity monitoring, paired SSC sampling, suspended sediment grain-size analysis, and controlled laboratory mixing experiments to construct and extend turbidity–SSC relationships in the Kuoqionggangri Glacier Basin. At the glacier terminus and basin outlet, paired field samples covered turbidity values up to 2840 NTU, whereas the turbidity sensors recorded values up to 5580 NTU. A single turbidity–SSC relationship fitted for each cross-section provided only moderate performance (R^2 = 0.85~0.86). After partitioning the observations into snowmelt-, glacier melt-, and rainfall-dominated periods, model performance generally improved (R^2 = 0.78~0.98), demonstrating the importance of process-based stratification for turbidity-based SSC estimation in glacier basins.

Direct extrapolation of period-specific turbidity–SSC relationships from the low turbidity range (<1400 NTU) to the medium turbidity range (1400–3000 NTU) performed poorly (NSE = -0.67 to 0.11), indicating that the fitted relationships were not directly transferable beyond the calibration segment. Laboratory mixing experiments showed that suspended sediment grain-size

https://doi.org/10.5194/egusphere-2026-4910
Preprint. Discussion started: 15 September 2026

composition was the dominant control on turbidity–SSC variability under contrasting runoff-supply conditions. Extrapolated turbidity–grain-size relationships performed well in the validation range (NSE = 0.91~0.98). By using the extrapolated grain-size composition at a given turbidity to prepare laboratory mixtures and derive the corresponding turbidity–SSC curve, SSC estimates were substantially improved (NSE = 0.96~0.98). This confirms that grain-size informed laboratory mixing experiments can extend turbidity–SSC relationships into high-turbidity ranges that are difficult to capture through field sampling alone.

The proposed framework can be generalized into four main steps: (1) continuous turbidity monitoring and paired SSC sampling should be conducted at representative cross sections to establish field-based turbidity–SSC relationships over the widest possible observational range; (2) monitoring records should be partitioned according to dominant hydrological processes; (3) suspended sediment samples from each period should be analyzed for key physical properties, such as grain-size distribution and organic-matter content, and their relationships with turbidity should be quantified; and (4) controlled laboratory mixing experiments should be used to generate turbidity–SSC curves for representative sediment characteristics, allowing SSC to be derived and validated beyond the range covered by paired field samples. In basins where organic matter, mineral composition, or particle shape varies substantially, these additional controls should be incorporated into the experimental design.

Because the present findings are based on a single glacier basin with specific hydroclimatic, geomorphic, and sediment source conditions, the broader applicability of the framework requires further evaluation. Future studies should apply this framework to a wider range of glacier basins and examine how glacier type, bedrock lithology, sediment source characteristics, and basin morphology influence turbidity–SSC relationships. More broadly, the results show that variations

https://doi.org/10.5194/egusphere-2026-4910
Preprint. Discussion started: 15 September 2026

in suspended sediment grain-size composition, generated by contrasting water and sediment production processes, are the principal cause of changes in turbidity–SSC relationships. The study therefore provides both a process-based explanation for the instability of conventional single curve calibrations and a practical framework for constructing and extending turbidity–SSC relationships in small glacier basins. These findings support improved monitoring and interpretation of suspended sediment dynamics in cold region rivers.

Data availability

The 10 min turbidity records used in this study were obtained from long-range, real-time turbidity monitoring systems installed at two hydrological cross-sections in the Kuoqionggangri Glacier Basin: the glacier terminus at 5316.8 m a.s.l. and the basin outlet at 4905.5 m a.s.l. The monitoring network was established by the Lhasa Earth System Multi-Dimensional Observatory Network (LESMDON). Background information on the basin and the classification of dominant hydrological periods is provided in Liu et al. (2025). Meteorological data were obtained from LESMDON and in situ rain-gauge measurements. Snow cover fraction data were derived from Moderate Resolution Imaging Spectroradiometer (MODIS) products accessed through the NASA National Snow and Ice Data Center (NSIDC; https://nsidc.org/home). Paired suspended sediment concentration samples used in this study are available from Mendeley Data at https://doi.org/10.17632/f9hb73t94n.1 (Liu, 2026).

Author contribution

CL: conceptualization, formal analysis, in vestigation, methodology, designed and carried out the experiments, visualization, writing draft. FZ: writing (review and editing), resources, funding acquisition. CZ: writing (review and editing), funding acquisition. SK: writing (review and editing).

https://doi.org/10.5194/egusphere-2026-4910
Preprint. Discussion started: 15 September 2026

Competing interests

The contact author has declared that none of the authors has any competing interests.

Acknowledgments

This study was supported by the National Natural Science Foundation of China (42125104, 42377340) and Lhasa Key Science and Technology Program (LSKJ202420).

References

Bakker, M., Legout, C., Biron, R., Nord, G., Le Bouteiller, C., Boithias, L., Camenen, B., Cotel, S., Coulaud, C., Denis, H., Dramais, G., Droujko, J., Fovet, O., Freche, G., Grippa, M., Le Coz, J., Lucas, A., Martinez, J. M., Meric, F., Mora, H., Némery, J., Payandi Rolland, D., Pierrefeu, G., Probst, A., Probst, J. L., Raclot, D., Ribolzi, O., Rousseau, C., Salvador Blanes, S., Santini, W., Seve, F., Thollet, F., Vanhooydonck, P., and Zanker, S.: Intercomparison of optical scattering turbidity sensors for a wide range of suspended sediment types and concentrations, Catena, 245, 108307, https://doi.org/10.1016/j.catena.2024.108307, 2024.

Bilotta, G. and Brazier, R.: Understanding the influence of suspended solids on water quality and aquatic biota, Water Res., 42, 2849-2861, https://doi.org/10.1016/j.watres.2008.03.018, 2008.

Birmachu, A., Feyissa, T., and Diriba, B.: Evaluation of the impacts of turbidity on Gilgel-Gibe I reservoir storage, Omo-Gibe river basin, Ethiopia, Heliyon, 10, e36294, https://doi.org/10.1016/j.heliyon.2024.e36294, 2024.

Bright, C. and Mager, S.: A national-scale study of spatial variability in the relationship between turbidity and suspended sediment concentration and sediment properties, River Res. Appl., 36, 1449-1459, https://doi.org/10.1002/rra.3679, 2020.

https://doi.org/10.5194/egusphere-2026-4910
Preprint. Discussion started: 15 September 2026

Bright, C., Mager, S., and Horton, S.: Response of nephelometric turbidity to hydrodynamic particle size of fine suspended sediment, Int. J. Sediment Res., 35, 444-454, https://doi.org/10.1016/j.ijsrc.2020.03.006, 2020.

Callesen, I., Keck, H., and Andersen, T. J.: Particle size distribution in soils and marine sediments by laser diffraction using Malvern Mastersizer 2000: method uncertainty including the effect of hydrogen peroxide pretreatment, J. Soils Sediments, 18, 2500-2510, 2018.

Chauché, N., Hubbard, A., Gascard, J.-C., Box, J. E., Bates, R., Koppes, M., Sole, A., Christoffersen, P., and Patton, H.: Ice–ocean interaction and calving front morphology at two west Greenland tidewater outlet glaciers, The Cryosphere, 8, 1457-1468, https://doi.org/10.5194/tc-8-1457-2014, 2014.

Chen, F., Cai, Q., Sun, L. Y., and Lei, T. W.: Discharge-sediment processes of the Zhadang Glacier on the Tibetan Plateau measured with a high-frequency data acquisition system, Hydrol. Process., 30, 4330-4338, 2016.

Choi, M., Ryu, J., and Ahn, J.: Analysis of the relationship between turbidity and benthic macroinvertebrate communities in the upper stream of Soyang River Dam, J. Korean Soc. Ecol. Infrastruct. Eng., 32, 123-135, 2024.

Chung, S. W., Jung, Y. R., Ko, I. H., and Kim, N. I.: Development and validation of a decision support system for the real-time monitoring and management of reservoir turbidity flows: a case study for Daecheong dam, J. Korea Water Resour. Assoc., 41, 293-303, https://doi.org/10.3741/JKWRA.2008.41.3.293, 2007.

Chung, S. W., Lee, H. S., and Jung, Y. R.: Turbidity modeling for a negative buoyant density flow in a reservoir with consideration of multiple particle sizes, J. Korean Soc. Water Environ., 24, 365-377, 2008.

Clifford, N. J., Richards, K. S., Brown, R. A., and Lane, S. N.: Laboratory and field assessment of an infrared turbidity probe and its response to particle size and variation in suspended sediment concentration, Hydrol. Sci. J., 40, 771-791, https://doi.org/10.1080/02626669509491464, 1995.

Davies-Colley, R. J., Ballantine, D. J., Elliott, S. H., Swales, A., Hughes, A. O., and Gall, M. P.: Light attenuation: a more effective basis for the management of fine suspended sediment than mass concentration, Water Sci.

https://doi.org/10.5194/egusphere-2026-4910
Preprint. Discussion started: 15 September 2026

Technol., 69, 1867–1874, https://doi.org/10.2166/wst.2014.096, 2014.

Davies-Colley, R. J. and Smith, D. G.: Turbidity, suspended sediment, and water clarity: a review, J. Am. Water Resour. Assoc., 37, 1085-1101, 2001.

Davies-Colley, R., Hughes, A. O., Vincent, A. G., and Heubeck, S.: Weak numerical comparability of ISO-7027-compliant nephelometers: ramifications for turbidity measurement applications, Hydrol. Process., 35, e14399, https://doi.org/10.1002/hyp.14399, 2021.

Delaney, I., Tedstone, A. J., Werder, M. A., and Farinotti, D.: Sediment transport capacity response to variations in water discharge in pressurized subglacial channels, The Cryosphere, 19, 2779–2795, https://doi.org/10.5194/tc-19-2779-2025, 2025.

De Lange, S. I., Sehgal, D., Martínez-Carreras, N., Waldschläger, K., Bense, V., Hissler, C., and Hoitink, A. J. F.: The impact of flocculation on in situ and ex situ particle size measurements by laser diffraction, Water Resour. Res., 60, e2023WR035176, https://doi.org/10.1029/2023WR035176, 2024.

Dethier, E. N., Erikson, C. M., and Renshaw, C. E.: Thaw slump erosion accelerates fluvial sediment transport after a heatwave on the Taymyr Peninsula, Russia, The Cryosphere, https://doi.org/10.5194/egusphere-2025-5691, 2025.

Downing, J.: Twenty-five years with OBS sensors: the good, the bad, and the ugly, Cont. Shelf Res., 26, 2299-2318, https://doi.org/10.1016/j.csr.2006.07.018, 2006.

Droujko, J. and Molnar, P.: Open-source, low-cost, in-situ turbidity sensor for river network monitoring, Sci. Rep., 12, 10341, https://doi.org/10.1016/j.csr.2006.07.018, 2022.

Druine, F., Verney, R., Deloffre, J., Lemoine, J., Chapalain, M., Landemaine, V., and Lafite, R.: In situ high-frequency long-term measurements of suspended sediment concentration in turbid estuarine system (Seine Estuary, France): optical turbidity sensors response to suspended sediment characteristics, Mar. Geol., 400, 24-37, 2018.

https://doi.org/10.5194/egusphere-2026-4910
Preprint. Discussion started: 15 September 2026

Felix, D., Albayrak, I., and Boes, M. R.: In-situ investigation on real-time suspended sediment measurement techniques: turbidimetry, acoustic attenuation, laser diffraction (LISST) and vibrating tube densimetry, Int. J. Sediment Res., 33, 3-17, https://doi.org/10.1016/j.ijsrc.2017.11.003, 2018.

Gippel, C. J.: Potential of turbidity monitoring for measuring the transport of suspended solids in streams, Hydrol. Process., 9, 83-97, https://doi.org/10.1002/hyp.3360090108, 1995.

Gray, J. R. and Gartner, J. W.: Technological advances in suspended-sediment surrogate monitoring, Water Resour. Res., 45, W00D29, https://doi.org/10.1029/2008WR007063, 2009.

Göransson, G., Larson, M., and Bendz, D.: Variation in turbidity with precipitation and flow in a regulated river system-river Göta Älv, SW Sweden, Hydrol. Earth Syst. Sci., 17, 2529–2542, https://doi.org/10.5194/hess-17-2529-2013, 2013.

Hoffmann, O. T., Baulig, Y., Fischer, H., and Blöthe, J.: Scale breaks of suspended sediment rating in large rivers in Germany induced by organic matter, Earth Surf. Dynam., 8, 661-678, https://doi.org/10.5194/esurf-8-661-2020, 2020.

Jalón-Rojas, I., Schmidt, S., and Sottolichio, A.: Turbidity in the fluvial Gironde Estuary (southwest France) based on 10-year continuous monitoring: sensitivity to hydrological conditions, Hydrol. Earth Syst. Sci., 19, 2805–2819, https://doi.org/10.5194/hess-19-2805-2015, 2015.

Kaless, G., Malnero, H., Frumento, O., and Pascual, M.: Rainfall and hydrograph styles in ephemeral streams of the drylands of Patagonia (South America-Argentina), Water Resour. Res., 60, e2024WR037601, https://doi.org/10.1029/2024WR037601, 2024.

Kim, J., Kwon, S., Chung, S., and Kim, Y. D.: Turbidity and suspended sediment relationship based on sediment composition and particle size distribution, Sci. Rep., 15, 16286, https://doi.org/10.1038/s41598-025-00435-2, 2025.

Knight, J. and Harrison, S.: Periglacial and paraglacial environments: a view from the past into the future, Geol.

https://doi.org/10.5194/egusphere-2026-4910
Preprint. Discussion started: 15 September 2026

Soc. Lond. Spec. Publ., 320, 1-4, https://doi.org/10.1144/SP320.1, 2009.

Kostaschuk, R., Nasr-Azadani, M. M., Meiburg, E., Wei, T. Y., Chen, Z. Y., Negretti, M. E., Best, J., Peakall, J., and Parsons, D. R.: On the causes of pulsing in continuous turbidity currents, J. Geophys. Res.-Earth, 123, 2827-2843, https://doi.org/10.1029/2018JF004719, 2018.

Landers, M. N. and Sturm, T. W.: Hysteresis in suspended sediment to turbidity relations due to changing particle size distributions, Water Resour. Res., 49, 5487-5500, https://doi.org/10.1002/wrcr.20394, 2013.

Li, D. F., Lu, X. X., Overeem, I., Walling, D. E., Syvitski, J., Kettner, A. J., Bookhagen, B., Zhou, Y. J., and Zhang, T.: Exceptional increases in fluvial sediment fluxes in a warmer and wetter High Mountain Asia, Science, 374, 599-603, https://doi.org/10.1126/science.abi9649, 2021a.

Li, J., Zhang, M., Jiang, E., Pan, L., Wang, A., Wang, Y., and Jian, S.: Influence of floodplain flooding on channel siltation adjustment under the effect of vegetation on a meandering riverine beach, Water, 13, 1402, https://doi.org/10.3390/w13101402, 2021b.

Li, H., Lv, J., He, X., Bao, Y., and Nsabimana, G.: Precipitation-dependent sensitivity of suspended sediment concentration to turbidity in a mountainous river in southwestern China, Ecol. Indic., 159, 111644, https://doi.org/10.1016/j.ecolind.2024.111644, 2024.

Li, Y., Zhang, T., Zhao, Y., Guo, Z., Han, P., Zhong, Q., Liu, L., Mao, S., Wang, Y., and Li, D.: Impact of climate change and vegetation greening on sediment transport in the Yarlung Tsangpo River, Catena, 261, 109557, https://doi.org/10.1016/j.catena.2025.109557, 2025.

Liu, M., Zhu, Y., Zhou, Z., and Sun, D.: Bimodal bed load transport characteristics under the influence of mixture ratio, Water, 15, 487, https://doi.org/10.3390/w15030487, 2023.

Liu, C., Zhang, F., Zeng, C., Zhao, Y., and Yang, W.: Dynamics of suspended sediment sources in the Kuoqionggangri glacier basin, Tibetan Plateau, under diverse hydrometeorological conditions, J. Hydrol., 660, 133510, https://doi.org/10.1016/j.jhydrol.2025.133510, 2025.

https://doi.org/10.5194/egusphere-2026-4910
Preprint. Discussion started: 15 September 2026

Mager, S. and Horton, S.: Particle size and geochemistry of suspended material and its influence on nephelometric turbidity, River Res. Appl., 41, 1300-1314, https://doi.org/10.1002/rra.4446, 2025.

Mathers, L. K., Rice, S. P., and Wood, P. J.: Discharge and suspended sediment time series as controls on fine sediment ingress into gravel river beds, Catena, 173, 253-263, https://doi.org/10.1016/j.catena.2018.10.001, 2019.

Merten, G. H., Capel, P. D., and Minella, J. P. G.: Effects of suspended sediment concentration and grain size on three optical turbidity sensors, J. Soils Sediments, 14, 1235-1241, https://doi.org/10.1007/s11368-013-0813-0, 2014.

Murillo-Bermúdez, L. F., Salustiano-Martim, A. L. S., Poleto, C., and Dalfré Filho, J. G.: Correlation of turbidity and suspended sediment concentration in natural water flow using alternative data of water treatment plant: case study in the upper Jundiaí River, Brazil, Int. J. River Basin Manag., 21, 233-241, https://doi.org/10.1080/15715124.2021.1961794, 2021.

Navratil, O., Esteves, M., Legout, C., et al.: Global uncertainty analysis of suspended sediment monitoring using turbidimeter in a small mountainous river catchment, J. Hydrol., 398, 246-259, https://doi.org/10.1016/j.jhydrol.2010.12.025, 2011.

Old, G. H., Lawler, D. M., and Snorrason, A.: Discharge and suspended sediment dynamics during two jökulhlaups in the Skaftá River, Iceland, Earth Surf. Process. Landf., 30, 1441-1460, https://doi.org/10.1016/j.jhydrol.2010.12.025, 2005.

Pfannkuche, J. and Schmidt, A.: Determination of suspended particulate matter concentration from turbidity measurements: particle size effects and calibration procedures, Hydrol. Process., 17, 1951-1963, https://doi.org/10.1002/hyp.1220, 2003.

Potes, M., Costa, M. J., and Salgado, R.: Satellite remote sensing of water turbidity in Alqueva reservoir and implications on lake modelling, Hydrol. Earth Syst. Sci., 16, 1623–1633, https://doi.org/10.5194/hess-16-

https://doi.org/10.5194/egusphere-2026-4910
Preprint. Discussion started: 15 September 2026

1623-2012, 2012.

Ravazzolo, D., Casasola, H., Fortesa, J., García Comendador, J., Cuello Llobel, F., Moragues, A., Company, J., and Estrany, J.: Bedload and suspended sediment transport analysis in a Mediterranean intermittent river, Catena, 267, 110009, https://doi.org/10.1016/j.catena.2026.110009, 2026.

Sehgal, D., Martínez-Carreras, N., Hissler, C., Bense, V., and Hoitink, A. J. F.: A generic relation between turbidity, suspended particulate matter concentration, and sediment characteristics, J. Geophys. Res.-Earth, 127, e2022JF006838, https://doi.org/10.1029/2022JF006838, 2022.

Sherriff, S. C., Rowan, J. S., Melland, A. R., Jordan, P., Fenton, O., and ÓhUallacháin, D.: Investigating suspended sediment dynamics in contrasting agricultural catchments using ex situ turbidity-based suspended sediment monitoring, Hydrol. Earth Syst. Sci., 19, 3349–3363, https://doi.org/10.5194/hess-19-3349-2015, 2015.

Skarbøvik, E., Gyritia Madsen van't Veen, S., Lannergård, E. E., Wenng, H., Stutter, M., Bieroza, M., Atcheson, K., Jordan, P., Fölster, J., Mellander, P.-E., Kronvang, B., Marttila, H., Kaste, Ø., Lepistö, A., and Kämäri, M.: Comparing in situ turbidity sensor measurements as a proxy for suspended sediments in north-western European streams, Catena, 225, 107006, https://doi.org/10.1016/j.catena.2023.107006, 2023.

Soulsby, C., Youngson, A., Moir, H., and Malcolm, I. A.: Fine sediment influence on salmonid spawning habitat in a lowland agricultural stream: a preliminary assessment, Sci. Total Environ., 265, 295–307, https://doi.org/10.1016/S0048-9697(00)00672-0, 2001.

Sutherland, T. F., Lane, P. M., Amos, C., and Downing, J.: The calibration of optical backscatter sensors for suspended sediment of varying darkness levels, Mar. Geol., 162, 587-597, https://doi.org/10.1016/S0025-3227(99)00080-8, 2000.

Voichick, N., Topping, D. J., and Griffiths, R. E.: Technical note: False low turbidity readings from optical probes during high suspended-sediment concentrations, Hydrol. Earth Syst. Sci., 22, 1767-1773,

https://doi.org/10.5194/egusphere-2026-4910
Preprint. Discussion started: 15 September 2026

https://doi.org/10.5194/hess-22-1767-2018, 2018.

Wang, Q., Fang, N. F., Zong, R. J., Zeng, Y., Dai, W., and Ni, L. S.: Climate change promotes universal increases in suspended sediment load of glacier-fed lakes on the Tibetan Plateau, Catena, 268, 110045, https://doi.org/10.1016/j.catena.2026.110045, 2026.

Walling, D. E.: Assessing the accuracy of suspended sediment rating curves for a small basin, Water Resour. Res., 13, 531–538, 1977.

Walling, D. E., Owens, P. N., and Leeks, G. J.: Fingerprinting suspended sediment sources in the catchment of the River Ouse, Yorkshire, UK, Hydrol. Process., 13, 955-975, 1999.

Woźniak, P. P. and Pisarska-Jamroży, M.: Debris flows with soft-sediment clasts in a Pleistocene glaciolacustrine fan (Gdansk Bay, Poland), Catena, 165, 178-191, https://doi.org/10.1016/j.catena.2018.01.022, 2018.

Woźniak, B. S., Stramski, D., Stramska, M., Reynolds, R. A., Wright, V. M., Miksic, E. Y., Cichocka, M., and Cieplak, A. M.: Optical variability of seawater in relation to particle concentration, composition, and size distribution in the nearshore marine environment at Imperial Beach, California, J. Geophys. Res.-Oceans, 115, C08027, https://doi.org/10.1029/2009JC005554, 2010.

Wu, J., Liu, Q., Liang, L., Yang, Y., Tang, Z., Qin, J., Li, S., Wang, X., and Li, C.: Can river damming amplify or dampen climate-driven changes in fluvial sediment transport? A case study of Jinsha River Basin, J. Hydrol., 664, 134446, 2026.

Wu, L., Qian, C., Sun, D., Wang, X., Zhao, X., and Shen, Y.: Development and application of a water resource assessment model with threshold-directed dynamic reward-penalty weighting in arid regions: a case study of the Shule River Basin, Northwest China, Appl. Water Sci., 16, 114, https://doi.org/10.1007/s13201-026-02806-0, 2026.

Yan, T., Gao, H., Chen, Y., Li, R., and Li, P.: Channel adjustments over 50 years in response to climate change and human activities in the Parlung Zangbo River, Tibetan Plateau, China, Earth Surf. Process. Landf., 50,

https://doi.org/10.5194/egusphere-2026-4910
Preprint. Discussion started: 15 September 2026

e70121, https://doi.org/10.1002/esp.70121, 2025.

Zeng, Y., Meng, X., Wang, B., Li, M., Chen, D., Ran, L., Fang, N., Ni, L., and Shi, Z.: Effects of soil and water conservation measures on sediment delivery processes in a hilly and gully watershed, J. Hydrol., 616, 128804, https://doi.org/10.1016/j.jhydrol.2022.128804, 2023.

Zhang, T., Li, D., East, A. E., Walling, D. E., Lane, S., Overeem, I., Beylich, A. A., Koppes, M., and Lu, X.: Warming-driven erosion and sediment transport in cold regions, Nat. Rev. Earth Environ., 3, 832-851, https://doi.org/10.1038/s43017-022-00362-0, 2022a.

Zhang, F., Zeng, C., Wang, G., Wang, L., and Shi, X.: Runoff and sediment yield in relation to precipitation, temperature and glaciers on the Tibetan Plateau, Int. Soil Water Conserv. Res., 10, 197–207, https://doi.org/10.1016/j.iswcr.2021.09.004, 2022b.

Ziegler, D. A., Benner, G. S., Tantasirin, C., Wood, S. H., Sutherland, R. A., Sidle, R. C., Jachowski, N., Nullet, M. A., Lu, X., Anond, S., Thomas, W. G., and Jefferson, M. F.: Turbidity-based sediment monitoring in northern Thailand: hysteresis, variability, and uncertainty, J. Hydrol., 519, 2020-2039, https://doi.org/10.1016/j.jhydrol.2014.09.010, 2014.